III.A.7 Characterization of Atomic and Electronic Structure of Electrochemically Active SOFC Cathode Surfaces

Objectives

- Investigate the atomic/electronic structures of various cathode materials using quantum chemical calculations.
- Predict the oxygen reduction mechanism on the surfaces of these cathode materials in a solid oxide fuel cell (SOFC).

Accomplishments

- The geometrical and electronic structures of the possible O_2 adsorption on the modeled surfaces of silver and CeO_2-supported silver have been predicted using density function theory (DFT) calculations. Results indicate that the adsorption of peroxide O_2^{2-} is more stable than that of superoxide O_2^- on silver surfaces.
- The mechanisms of O_2 reduction and oxygen ion transport on the modeled surfaces of silver and CeO_2-supported silver have been predicted from the computed potential energy surface (PES). Results suggest that oxygen reduction is more energetically favorable on the CeO_2-supported silver surface than on unsupported silver surfaces.
- The effective charges of the intermediate oxygen species on different silver surfaces have also been estimated from DFT calculations.

Introduction

The interaction of oxygen molecules with oxide-supported metal surfaces is considered as one of the modern classics of heterogeneous reactions for fuel cell and catalytic applications [1,2]. The reduction processes of oxygen molecules on the metal/oxide interface, which correspond to the electrode/electrolyte system, are the key reactions in the cathode region of SOFCs. The oxygen reduction process may occur via three parallel reaction routes, depending on the ionic and electronic transport properties of the cathode and electrolyte materials [3,4]. In the first route, oxygen molecules are adsorbed on the triple-phase boundary (TPB), where the electrolyte, electrode, and oxygen gas meet, and the reduced oxygen ions can directly combine with oxygen vacancies in the electrolyte. In the second route, oxygen molecules are adsorbed and dissociated on the cathode surface, which is a two-phase boundary (2PB), followed by the transport of the dissociated oxygen ions through the cathode to the electrolyte or along the surfaces of the cathode to the TPB. In the third route, oxygen molecules are adsorbed and/or dissociated on the electrolyte 2PB surface, followed by the transport of the adsorbed/dissociated oxygen ions along the surfaces of the electrolyte to the TPB, where they are reduced and incorporated into the electrolyte. For SOFCs with metallic electrodes, it is generally believed that oxygen reduction occurs predominantly at the TPB since metal electrodes are electronic conductors rather than ionic conductors. Nevertheless, the detailed mechanism of oxygen-metal/oxide interaction is still not well understood, and many fundamental concepts at the microscopic level remain unclear.

Meilin Liu (Primary Contact), Jeng-Han Wang
Georgia Institute of Technology
771 Frest Drive
Atlanta, GA 30332
Phone: (404) 894-6114; Fax: (404) 894-9140
E-mail: meilin.liu@mse.gatech.edu
Website: http://www.prism.gatech.edu/~ml44/liu.htm

DOE Project Manager: Lane Wilson
Phone: (304) 285-1336
E-mail: Lane.Wilson@netl.doe.gov

Approach

The electronic calculation to identify the intermediate and transition states in the oxygen reduction process on the 2PB and TPB is optimized by the spin-polarized DFT with the projector-augmented wave method (PAW) [5,6]. The exchange-correlation function is treated with the generalized gradient approximation (GGA) of PW91 formulation [7] for the total energy calculations. The Brillouin zone is sampled by the Monkhorst-Pack scheme [8].

The 2PB is modeled by Ag(111) and Ag(110) surfaces, which are constructed by 6-layer (111) and (110) slabs. Both the (111) and (110) slabs have 2×2 surface cells with 4 Ag atoms. The Monkhorst-Pack k-points, applied for the super cells of Ag(111) and Ag(110) surfaces, are set as 8×8×1 along $(11\bar{2})$ x $(1\bar{1}0)$ x (111) and 8×4×1 along $(1\bar{1}0)$ x (001) x (110) directions, respectively. The cutoff energy and vacuum space are kept at 400 eV and 10 Å, respectively. The top three layers are relaxed and the bottom three layers are fixed at the computed lattice constant during the structure optimization. The TPB is modeled by one Ag

monolayer covered on Ce- or O-terminated CeO_2(111) surfaces. The CeO_2(111) surface is constructed by a p(2x2) 9-layer slab with 12 [CeO_2] units. The top three layers are relaxed, the Monkhorst-Pack k-points are set as 3×3×1 along (211) x (011) x (111) directions, and a 10-Å vacuum space is presented along the (111) direction during the calculation.

Results

O_2 Adsorption: Calculations of adsorption energy suggest that the adsorptions on atop sites are less stable than those on 3-fold hollow sites, which can be rationalized from their bonding structures. Each adsorbed O_2 at the atop position forms one chemical bond with a single Ag atom; in contrast, the adsorbed O_2 at the 3-fold hollow site forms more bonds with nearby Ag atoms. The calculations also suggest that the side-on adsorbed O_2^{2-}(a) is more stable than the end-on adsorbed O_2^{-}(a). In the end-on adsorption of superoxide, only one O atom bonds with the surface, while in side-on adsorption of peroxide, both O atoms bond with the surface Ag atoms. The trends are consistent with the results of previous experimental observations [9,10].

The analysis of the bond lengths indicates that, first, all adsorbed O_2(a) has longer bond lengths than that in the gas phase, 1.236 Å; second, the adsorbed O_2(a) with longer bond lengths has higher adsorption energies because the adsorbate can donate more electrons and form stronger Ag–O bonds to stabilize the whole system. Therefore, the overall stability can be attributed to the energy produced by forming strong Ag–O bonds, which is more than the energy consumed by partially breaking the O–O bond.

The vibration frequencies of the most stable superoxide and peroxide on the modeled TPB, atomic Ag covered on Ce- and O-terminated CeO_2(111) surface, were computed. The adsorptions of superoxide forms with shorter O–O bonds have higher vibration frequencies (1003–1079 cm^{-1}) than those of peroxide forms (750–916 cm^{-1}). The O–O vibrations on the modeled TPB are closer to the experimental observations of O_2(a) on the pure CeO_2(111) surface, O_2^{-}(a): 1127–1135 cm^{-1} and O_2^{2-}(a): 831–877 cm^{-1} (11), than to those of O_2(a) on metal surfaces, O_2^{-}(a): 870–1020 cm^{-1} and O_2^{2-}(a): 610–660 cm^{-1} [12]. This implies that the Ag-covered CeO_2 surfaces still retain the surface properties of CeO_2(111) rather than those of silver surfaces.

O_2 Reduction: The reduction process is related to the O-O dissociation process from the most stable O_2(a) adsorption. On the modeled TPB of Ag-covered O-terminated CeO_2(111) surface, the transition state of the O_2 reduction process has a 0.43-eV reaction barrier when the O-O bond is extended to ~2 Å. The resulting product of the two dissociated O(a) prefers being adsorbed on the two nearest 3-fold hollow sites with an exothermicity of -0.44 eV. On the other modeled TPB of Ag-covered Ce-terminated CeO_2(111) surface, the O_2 reduction process has a 0.28-eV reaction barrier. The dissociated O atoms prefer bonding with subsurface Ce compared to surface Ag atoms with a much higher exothermicity of 4.70 eV because the adsorption energies on atop sites of O–Ce (5.55 eV) are much higher than that of O–Ag (1.99 eV). The potential energy surface (PES) with Bader charge [13] analysis of this process is shown in Figure 1. As a result, the reduction processes on the two modeled TPBs have low reaction barriers and are highly exothermic.

On the other hand, the reduction processes on the modeled 2PB of Ag(111) and Ag(110) surfaces have 0.85-eV and 0.60-eV reaction barriers, respectively. The PES of the O_2 dissociation process on the Ag(111) surface with Bader charge analysis, for example, is shown in Figure 2. Unlike the TPB cases, the reduction

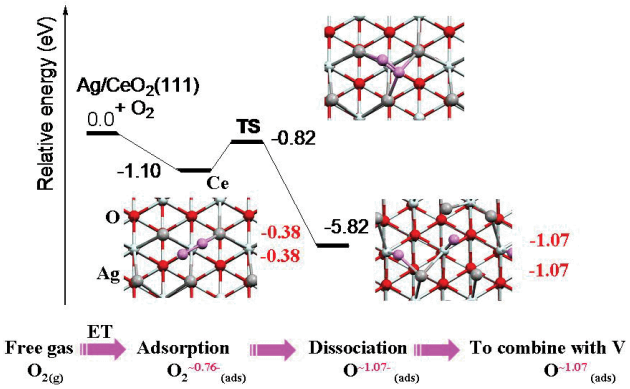

FIGURE 1. PES and geometrical structures of O_2(a) → 2O(a) dissociation processes on a Ag-covered, Ce-terminated, CeO_2(111) surface. The black numbers are the relative energies referenced to O_2(g)/surfaces (= 0). The red numbers are the Bader charges of the adsorbed O.

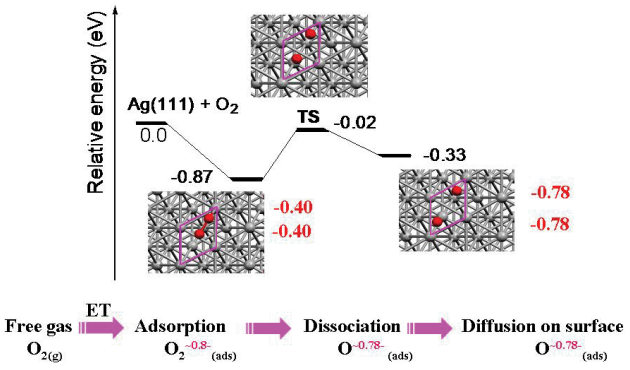

FIGURE 2. PES and geometrical structures of O_2(a) → 2O(a) dissociation processes on a Ag(111) surface. The black numbers are the relative energies referenced to O_2(g)/surfaces (= 0). The red numbers are the Bader charges of the adsorbed O.

processes on the modeled 2PB are endothermic, 0.54 eV on Ag(111) and 0.25 eV on Ag(110) surfaces. Therefore, from the mechanism calculations, the O_2 reduction process is energetically more favorable to occur on the TPB than on the 2PB since the process has a lower reaction barrier and higher exothermicity on the TPB.

Oxygen Ion Transport: The O ion transport refers to the motion of the dissociated O(a) from one stable site to another on the surface. Compared with surface morphology, the separation between the stable sites on the TPB is larger than that on the 2PB. Compared with the electronic structure, the subsurface atoms of the TPB have stronger interaction with surface O(a) than those of the 2PB. Therefore, the transport process near the TPB of Ag supported by the O-terminated CeO_2(111) surface has a higher energy barrier (~0.59 eV) than on the 2PB of silver: the Ag(111) surface has a barrier of 0.37 eV and the Ag(110) surface has a barrier of 0.17 eV. On the other modeled TPB of Ag supported by Ce-terminated CeO_2(111) surface, the O ions transport from the surface Ag layer directly to the subsurface Ce without any barrier and with a high exothermicity of -3.56 eV. This result suggests that any dissociated O at the TPB will be dragged into the unsaturated Ce^{3+} in the electrolyte quickly.

These calculations predict that the TPB of Ag supported by the Ce-terminated CeO_2(111) surface has the lowest energy barrier for O_2 reduction, and the dissociated O ions can directly transport to the CeO_2 bulk without any energy barrier, implying that the TPBs are the most active sites for oxygen reduction. This result agrees well with the experimental observation that cell performance can be enhanced by increasing the TPB area [14,15].

Conclusions and Future Directions

Oxygen-reduction mechanisms on silver-based cathodes have been examined by spin-polarized DFT calculation with the PAW method. The stepwise reactions occurring on a silver-based SOFC cathode can be described as

$$O_2(g)\ (+\ e) \rightarrow O_2^-\ (+\ e) \rightarrow O_2^{2-} \rightarrow 2O^{2-}\ (+V_o^{\bullet\bullet}) \rightarrow O_o^x$$

where $V_o^{\bullet\bullet}$ represents an oxygen vacancy in the electrolyte and O_o^x corresponds to an oxygen ion at a regular oxygen site in the electrolyte.

The computed energies of these reactions, as summarized in Figure 3, show that the cathodic reactions in an SOFC, the O_2 adsorption, dissociation, and reduction as well as the combination of the dissociated O ions with oxygen vacancies in the electrolyte are energetically more favorable to take place in the TPB region where subsurface Ce atoms are present (together with oxygen vacancies). This prediction is consistent with the experimental

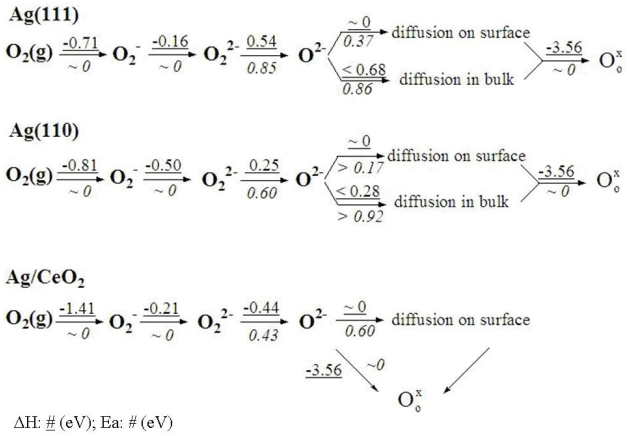

FIGURE 3. The stepwise reaction mechanisms of oxygen reduction processes on Ag(111) and Ag(110) surfaces and at a TPB, silver-covered, Ce-terminated CeO_2(111) surface. The underlined numbers represent the heat of reaction, ΔH, in eV whereas the italic numbers represent the reaction barrier, Ea, in eV.

observations that the efficiency of a SOFC can be enhanced by increasing the TPB areas.

Future studies are briefly outlined as follows:

- Predict O_2 reduction mechanisms on different cathode materials using similar approaches.
- Take into consideration the effect of temperature and pressure in the calculations to predict the catalytic activity of different cathode materials under various conditions.
- Take into consideration the effect of an applied direct current polarization in the calculations to simulate practical SOFC operating conditions.

FY 2006 Publications/Presentations

1. J. H. Wang, M. Liu, M. C. Lin, Oxygen reduction reactions in the SOFC cathode of Ag/CeO_2; *Solid State Ionics.* **177**, 939 (2006).

2. J. H. Wang, M. Liu, Catalytic ability in Ag electrode and Ag/CeO_2 triple phase boundary, to be submitted.

3. J. H. Wang, M. Liu, Mechanism of Oxygen Reduction on a Ag/CeO_2 Based SOFC Cathode; Strategic Energy Initiative (SEI) Energy Research Exposition, Atlanta, GA, February 28th, 2006.

References

1. M.S. Chen, D.W. Goodman, Science 306 (2004) 232.

2. C.T. Campbell, Science 306 (2004) 234.

3. M. Liu and J. Winnick, "Fundamental Issues in Modeling of Porous Electrodes of Mixed Ionic-Electronic Conductors", *Solid State Ionics*, Vol. **118** (1999) 11-21.

4. J. Fleig, Annual Review of Materials Research 33 (2003) 361.

5. P.E. Blöchl, Physical Review B 50 (1994) 17953.

6. G. Kresse, D. Joubert, Physical Review B 59 (1999) 1758.

7. J.P. Perdew, J.A. Chevary, S.H. Vosko, K.A. Jackson, M.R. Pederson, D.J. Singh, C. Fiolhais, Physical Review B 46 (1992) 6671.

8. H.J. Monkhorst, J.D. Pack, Physical Review B 13 (1976) 5188.

9. M.R. Salazar, C. Saravanan, J.D. Kress, A. Redondo, Surface Science 449 (2000) 75.

10. H. Nakatsuji, H. Nakai, Chemical Physics Letters 197 (1992) 339.

11. V.V. Pushkarev, V.I. Kovalchuk, J.L. d'Itri, Journal of Physical Chemistry B 108 (2004) 5341.

12. R.D. Jones, D.A. Summerville, F. Basolo, Chemical Reviews 79 (1979) 13.

13. R.F.W. Bader, Atoms in Molecules - A Quantum Theory, Oxford, Oxford University Press, 1990.

14. T. Horita, K. Yamajia, N. Sakaia, Y. Xionga, T. Katoa, H. Yokokawa, T. Kawada, Journal of Power Sources 106 (2002) 224.

15. R. Radhakrishnan, A.V. Virkar, S.C. Singhalb, Journal of The Electrochemical Society 152 (2005) A927.